Active responsive colloids coupled to different thermostats

Polina Gaindrik,[1] Upayan Baul,[1] and Joachim Dzubiella[1,2,*]

[1]*Applied Theoretical Physics–Computational Physics, Physikalisches Institut, Albert-Ludwigs-Universität Freiburg, D-79104 Freiburg, Germany*

[2]*Cluster of Excellence livMatS @ FIT–Freiburg Center for Interactive Materials and Bioinspired Technologies, Albert-Ludwigs-Universität Freiburg, D-79110 Freiburg, Germany*

(Received 31 January 2022; accepted 12 July 2022; published 26 July 2022)

We introduce a model of active responsive colloids (ARCs) in which an internal degree of freedom (DoF) of a single colloidal particle is "activated" by coupling it to a different thermostat than for the translational DoFs. As for the responsive internal DoF, we consider specifically the size (diameter) of the spherical particles, which is confined by a harmonic parent potential being either entropic or energetic in nature. The ARCs interact via a repulsive Hertzian pair potential, appropriate to model hydrogels or elastic colloids, and are studied for various densities using Brownian dynamics simulations. We tune the internal activity in the nonequilibrium steady state by scanning through a wide range of internal temperatures, both smaller ("colder") and larger ("hotter") than the translational temperature. The results show a rich and intriguing behavior for the emergent property distributions, colloidal pair structure, and the diffusive translational dynamics controlled by the internal activity, substantially depending on whether the internal DoF moves in an entropic or energetic potential. We discuss theoretical thermal limits and phenomenological models which can explain some of the nonequilibrium trends qualitatively. Our study indicates that particle dynamical polydispersity as well as the structure and dynamics of dense macromolecular suspensions can be vastly tuned by internal activity in terms of internal "hot" or "cold" fluctuating states.

DOI: 10.1103/PhysRevE.106.014613

I. INTRODUCTION

Living materials rely on nonequilibrium processes driven by internal fueling, e.g., by irreversible ATP or GTP consumption. Based on dynamical self-assembly, sensing, and collective signaling and feedback, biological systems possess autonomous and adaptive behavior, not yet achievable with static man-engineered systems [1,2]. A prominent example is the bacterial *quorum sensing*, which is the self-regulation of internal gene expression rates in response to fluctuations in overall cell-population density [3] or environmental (e.g., antibiotic) stress [4,5]. These fascinating active and collective nonequilibrium processes are inspiring for the design of "intelligent" synthetic materials to potentially mimic living systems for advanced function, such as a programmable time response and adaptive feedback [2,6,7].

Of high potential for biomimetic material design are polymer-based *responsive* systems that change their conformation and function in response to external stimuli. Specific examples embrace thin polymer films and brushes as well as stimuli-responsive microgels that have already diverse application, such as smart coatings, sensors, motile micromachines [8], cell capsules in tissue engineering and for drug delivery [9–11], or colloidal nanoreactors sheltering internal chemical reactions [12]. The external stimulus can be achieved with temperature [13], pH [14,15], osmotic pressure (crowding) [16], electromagnetic fields, light, or the presence of certain enzymes or ions [17]. The response is expressed in reversible or irreversible swelling or collapse, change in shape and structure, aggregation, and adsorption of the polymeric aggregates [9,18]. In particular, the colloid-polymer duality of soft microgel particles [19–21] and their stimuli-triggered conformational switching [9] open new avenues for creating active and programmable colloid-based fluids and materials.

In order to build a theoretical framework for active and responsive colloidal dispersions, recently the model of *responsive colloids* (RCs) was presented [22]. There, in addition to the conventional effective pair potential, a "property" as an internal degree of freedom (DoF) was introduced as a collective variable, living on its own parent energy landscape. Using Brownian dynamics computer simulations, it was shown—using the colloidal size as the responsive DoF—how such a dynamical polydispersity affects the structure and dynamics of RC suspension due to the emerging response and many-body correlations [23]. Moreover, it was demonstrated by using a bimodal parent distribution how the populations and the transition kinetics of the stochastic two-state switching of a RC is modified collectively by spatial packing and crowding [24]. Similar models introducing internal DoFs have been used to study, e.g., compressibility effects in polymer and microgel systems [25–27], conformational effects in protein dispersions [28–30], or soft glasses [31,32].

The aim of this work is to move one step forward towards living systems and extend the RC model to include internal (nonmotile) activity, thereby introducing the active

*Corresponding author: joachim.dzubiella@physik.uni-freiburg.de

RC (ARC) model. As opposed to active Brownian particles (ABPs) [33,34], where active motility (e.g., swimming by self-propulsion) is considered, our aim is to activate an internal DoF of the responsive colloids, such as their size, shape, dipole, etc. [22] In mind we have a model for "living" colloids, e.g., bacteria or a colloids with an internal "engine," provided, for example, by a chemical reaction, which is driven locally, such that energy transduction occurs at the particle scale [35] and internal fluctuations are decoupled from those of the translational bath. Concrete examples could be nanoreactors of core-shell or yolk-shell architecture [12] where small metal nanoparticles in the center of a large (hydrogel) colloid catalyze exothermic chemical reactions and locally produce heat. Alternatively, the nanoparticles can be heated by external light sources [36,37]. The heat dissipates away on the colloidal length scale [38] and internal and external temperature baths may have significantly different temperatures in the stationary state. Another example could be complex feedback reactions in colloids which govern the internal size fluctuations instead of the external heat bath [39].

As the simplest route to activate the internal DoF, motivated by recent developments in literature [35,40–47], we use the *internal temperature* as the active control parameter. In other words, we suggest to couple the internal property DoF to a different thermostat than the translational DoFs of the RCs, and we tune the internal DoF between "cold" and "hot" behavior with respect to the translational heat bath. The augmented thermal fluctuations then lead to violations of the fluctuation-dissipation balance in the system [48], driving it out of equilibrium. We want to fundamentally understand the consequences of such an activity on the structure and dynamics of interacting active colloidal dispersions.

To achieve this goal, we modify the previous equilibrium RC model [23] with the particle size fluctuating in a harmonic parent potential, by a two-temperature dynamics with the translational motion and the internal DoF coupled to different thermostats in an overdamped Brownian dynamics (BD) framework. We employ a Hertzian pair potential as a generic form for soft-repulsive colloids, such as microgels in the swollen state [49–52]. The system is then investigated using numerical BD simulations for different ratios between the translational and property temperatures. We study the structural and dynamical properties of two different RCs models: an "entropic model" in which the parent energy landscape scales linearly with internal temperature (and single-particle size distributions remain unaffected by internal temperature changes) and an "energetic model" in which the parent landscape is purely energetic. As results, we find a rich and intriguing behavior of the structure and dynamics of the systems, demonstrating the power of control the internal activity has on collective properties. Previous works on two-temperature models showed that for simple symmetric Hamiltonians one can introduce the concept of an effective temperature to describe stationary distributions in nonequilibrium [35,40,42–48]. Inspired by these works we attempt phenomenological interpretations of our observations which should be useful to establish a complete theory of ARCs and help guiding experimental synthesis in future works.

II. METHODS

A. Active responsive colloid (ARC) model

As in our previous work in equilibrium [23], we consider a system of N RCs with coordinates $\mathbf{r}^N$ and sizes σ^N in a fixed volume V, obeying the Hamiltonian

$$H(\mathbf{r}^N, \sigma^N) = \sum_{i}^{N} \psi(\sigma_i) + \frac{1}{2} \sum_{i \neq j}^{N} \phi(\mathbf{r}_i, \mathbf{r}_j; \sigma_i, \sigma_j), \quad (1)$$

where $\psi(\sigma_i)$ is the single-particle property potential acting on particle i, and $\phi(\mathbf{r}_i, \mathbf{r}_j; \sigma_i, \sigma_j)$ is the pairwise interaction potential between particles i and j. We define $\rho = N/V$ as the number density of our system.

The property potential defines the parent energy landscape which confines the size σ_i of each particle within a harmonic potential with a lower bound, according to

$$\psi(\sigma_i) = \begin{cases} \frac{1}{2} k_\sigma (\sigma_i - \sigma_0)^2, & \text{if } \sigma > 0 \\ \infty, & \text{if } \sigma \leqslant 0, \end{cases} \quad (2)$$

where the spring constant k_σ defines the strength of the potential and σ_0 is the (global) minimum of the potential and sets our unit length scale. Since σ describes the particle size, we restrict it only to assume positive values. However, k_σ will be chosen relatively stiff such that the hard boundary $\sigma > 0$ affects only a very small part of the Gaussian single-particle size manifestations. We therefore also safely treat σ_0 as the mean size of a single particle.

The interaction potential $\phi(\mathbf{r}_i, \mathbf{r}_j; \sigma_i, \sigma_j)$ is chosen corresponding to the RC model for soft and responsive microgels [49–52]: the pairwise interaction potential depends on the distance between two particles, $r_{ij} = |\mathbf{r}_i - \mathbf{r}_j|$, and is presented via the soft-repulsive Hertzian potential:

$$\phi(r_{ij}, \sigma_{ij}) = \epsilon \left(1 - \frac{r_{ij}}{\sigma_{ij}}\right)^{\frac{5}{2}} \Theta\left(1 - \frac{r_{ij}}{\sigma_{ij}}\right), \quad (3)$$

where $\sigma_{ij} = (\sigma_i + \sigma_j)/2$ according to the Lorentz combining rule, $\Theta(1 - r_{ij}/\sigma_{ij})$ is the Heaviside step function, and $\epsilon = 500\, k_B T_0$ determines the strength of the repulsion in units of our thermal energy scale $k_B T_0$. The Hertzian potential of such a form and energy shows good agreement with experimental results for soft-repulsive uncharged colloids in the swollen state [50–52] and also is applicable for soft microgels at small deformations and packing fractions up to unity [49]. It might be also a good model for elastic spherical bacteria for small deformations [53].

In contrast to our equilibrium work [23], however, we consider in this work that the property σ is in contact with a hypothetical bath of temperature T_σ and the translational DoFs are in contact with a bath with temperature T_0. Hence, all cases $T_\sigma \neq T_0$ with nonvanishing T_σ are nonequilibrium situations, and for $T_\sigma = T_0$ we recover the standard NVT_0 canonical ensemble. In our work, we set T_0 as reference scale (unit) and vary T_σ in units of T_0 from 0.1 to 10, thus scanning two orders of magnitude of the temperature ratio.

B. Temperature-dependence of the single-particle property distribution

Two different versions of the property potential $\psi(\sigma)$ are of particular interest in this work:

(1) *Entropic model:* In the entropic model, we consider that the property potential $\psi(\sigma)$ is directly proportional to the property temperature T_σ. The parameter k_σ in the parent potential Eq. (2) is then defined as $k_\sigma = k_B T_\sigma/\delta_0^2 \propto T_\sigma$, where δ_0 is the standard deviation of the corresponding property distribution, explicitly discussed below. We call it an "entropic model" because the temperature scales out in the Boltzmann distribution and the variation of the internal temperature does not affect the size distributions of a single, isolated particle.

(2) *Energetic model:* In the energetic model, the property potential $\psi(\sigma)$ does not depend on the property temperature T_σ. We assume the potential to be proportional to the fixed reference T_0 temperature: $k_\sigma = k_B T_0/\delta_0^2 \propto T_0$. In contrast to the entropic model, the single-particle size distributions will substantially (according to the Boltzmann weight) depend on T_σ.

With these premises, the property potential ψ then leads to the (normalized) property parent distribution for an isolated particle, $p(\sigma) \sim \exp[-\beta_\sigma \psi(\sigma)]$ with $\beta_\sigma = 1/k_B T_\sigma$, that is, explicitly

$$p(\sigma) = \frac{1}{\sqrt{2\pi\delta^2}} \exp\left[-\frac{1}{2}\left(\frac{\sigma-\sigma_0}{\delta}\right)^2\right]. \tag{4}$$

In the entropic model, the parent distribution $p(\sigma)$ stays the same for different T_σ with the standard deviation $\delta \equiv \delta_0$. In the energetic model, however, the distribution has a standard deviation dependent on the σ temperature via $\delta = \delta(T_\sigma) = \sqrt{T_\sigma/T_0}\delta_0 \sim \sqrt{T_\sigma}$. In words, the distribution peaks become sharp at σ_0 for $T_\sigma \to 0$. For all simulations we use $\delta_0 = 0.2\sigma_0$.

In dense suspensions, interactions will modify the parent size distributions and we obtain the density-dependent *emergent distribution*, $N(\sigma)$ [22,23]. (They will be presented in the Results section as an outcome of the simulations.) In the low-density limit (LDL, $\rho \to 0$), we have $N(\sigma) \to p(\sigma)$, i.e., we recover the parent distributions.

C. Double-thermostatted Brownian dynamics simulations

The evolution of the position coordinates $\mathbf{r} = \{x, y, z\}$ and the property σ of one particle i is determined by Brownian dynamics equations in the discrete form

$$\mathbf{r}_i(t+\Delta t) = \mathbf{r}_i(t) + \frac{\boldsymbol{f}^{\text{pair}}_{\mathbf{r},i}}{\zeta_\mathbf{r}(t)}\Delta t + \sqrt{\frac{2k_B T_0 \Delta t}{\zeta_\mathbf{r}(t)}}\boldsymbol{\eta}_\mathbf{r}$$

$$\sigma_i(t+\Delta t) = \sigma_i(t) + \frac{f_{\sigma,i}}{\zeta_\sigma}\Delta t + \sqrt{\frac{2k_B T_\sigma \Delta t}{\zeta_\sigma}}\eta_\sigma, \tag{5}$$

where Δt is the time step of the simulation; $\zeta_\mathbf{r}(t) = \zeta_0\sigma(t)/\sigma_0$ and $\zeta_\sigma = \zeta_0$ are the friction constants for the position coordinate and property, respectively. We assume Stokes friction for the translation and that the friction depends dynamically on the instantaneous particle size [23,24,54]. Hence, only in the special case $\sigma(t) = \sigma_0$, the viscous dynamics of the position and the property of a colloid are set by the same friction constant. To prevent the appearance of negative σ values, we reject BD moves if the particle size after one BD step $\sigma_i\ (t + \Delta\, t)$ is less than $0.05\sigma_0$ (which are very rare events) [23].

Moreover, T_0 and T_σ are the temperatures for the position coordinates and property evolution, respectively; $\eta_\mathbf{r}$ and η_σ are random variables drawn from the Gaussian distribution with zero mean and unit variance. Translation and property on their own obey the fluctuation dissipation theorem [55], and we assume them to be not correlated. All the random forces in Eqs. (5) thus represent white noise uncorrelated for different particles i, j and different times t, t' $\langle \eta_i(t)\eta_j(t')\rangle = \delta_{ij}\delta(t-t')$ [56,57]. Our time unit is the Brownian time scale τ_B, setting the single-particle diffusion of a particle with unit size σ_0 to $D_0 = \sigma_0^2/\tau_B$. The BD equations (5) together with Hamiltonian (1) completely define our nonequilibrium two-temperature ARC model, analogously to previous works on DoFs coupled to different thermostats [35,42,44].

The force acting on the position coordinates of the ith particle, $\boldsymbol{f}^{\text{pair}}_{\mathbf{r},i}$, is calculated as the gradient of the energy function and consists of the pairwise interaction term:

$$\boldsymbol{f}^{\text{pair}}_{\mathbf{r},i} = -\nabla_i H = -\nabla_i \sum_j \phi(r_{ij}, \sigma_{ij}). \tag{6}$$

The force acting on the property DoF, $f_{\sigma,i}$, describes the property evolution and consists of contributions from both single-particle property potential ψ and pair potential ϕ:

$$f_{\sigma,i} = -\frac{\partial H}{\partial \sigma_i} = f^{\text{single}}_{\sigma,i} + f^{\text{pair}}_{\sigma,i}, \tag{7}$$

where the first term is $f^{\text{single}}_{\sigma,i} = -\partial\psi(\sigma_i)/\partial\sigma_i$ and the second one is $f^{\text{pair}}_{\sigma,i} = -\sum_j \partial\phi(\sigma_i)/\partial\sigma_i$.

In our simulations, we scan through various property temperatures and ARC number densities ρ and calculate averages of distributions of sizes and coordinates. In particular, we calculate the emergent size distributions, $N(\sigma;\rho)$ [22,23], as well as conventional radial (pair) distribution functions (RDFs) as a function of particle pair distances r, $g(r;\rho)$ [22,23,56]. We finally also investigate the long-time diffusive behavior of the colloids. All values of the parameters used in the model and simulations are presented in Table I.

III. THERMAL LIMITS AND PHENOMENOLOGICAL MODEL

A. Thermal limits in the entropic model

It is at this point instructive for our understanding to consider the thermal limits of the internal temperature,

$$\text{(i)}\ \ T_\sigma \to 0 \quad \text{and} \quad \text{(ii)}\ \ T_\sigma \to \infty, \tag{8}$$

in the BD equations (5). Recall first that the parent distribution, $p(\sigma)$, per definition in the entropic model is not affected by the variation of T_σ. Hence, (i) and (ii) do not affect $p(\sigma)$ for the single particle and should also be of little effect in the LDL of the suspension. For the interacting case, pair forces from the surrounding come into play: In the limit (i) both the fluctuations and the property force f^{single}_σ vanish in the BD equation for the size σ. As a consequence, $\dot\sigma \propto f^{\text{pair}}_\sigma$ becomes dominant, and any two- or many-body repulsive interaction

TABLE I. List of parameters and their values used in the ARC model systems in the Brownian dynamics simulations.

Parameter		Value
Number of particles	N	512
Time step	Δt	$10^{-4}\tau_{\mathrm{BD}}$
Equilibration run	N_{eq}	10^6 steps
Production run	N_{prod}	10^7 steps
Number of saved steps	N_{save}	10^4 steps
Unit size	σ_0	1.0
Mean of $p(\sigma)$	σ_0	1.0
Reference standard deviation	δ_0	0.2
Reference friction value	ζ_0	1.0
Reference temperature	T_0	1.0
Energy unit	k_BT_0	1.0
Hertzian energy	ϵ	500.0
Property temperature	T_σ	0.1, 0.2, 0.5, 1.0, 2.0, 5.0, 10.0
Density	$\rho\sigma_0^3$	0.02, 0.2, 0.6, 0.95, 1.3, 1.7, 2.0

will easily compress the particle to small sizes. Hence, we expect to observe distributions with decreasing mean size for decreasing T_σ. In sufficiently dense systems where all particles are within their range of repulsive interactions, the pair forces lead strictly to $\dot{\sigma} < 0$, and in the absence of size fluctuations, the system eventually approaches ideal gas behavior for $T_\sigma \to 0$.

Conversely in the case of (ii), $T_\sigma \to \infty$, the pair forces become irrelevant and $\dot{\sigma} \propto f_\sigma^{\mathrm{single}}$ dominates. As a result, the translational and property dynamics in Eqs. (5) decouple. The system then samples an equilibrium of particles strictly following their parent distributions, as in conventional (non-responsive) polydisperse equilibrium systems [23]. Hence, while not providing rigid mathematical proofs at this stage, our inspection of the BD equations indicates the remarkable behavior that the internal temperature T_σ in the entropic model interpolates between two very different equilibrium systems, the ideal gas and conventional polydisperse behavior for $T_\sigma \to 0$ and $T_\sigma \to \infty$, respectively. The simulated distributions presented further below will indeed support these predictions.

B. Thermal limits in the energetic model

In the energetic model, the single-particle parent distribution, $p(\sigma)$, changes substantially with T_σ as discussed above and should be expressed in the dilute suspensions. For colder systems, the size distribution becomes sharp, for hot systems broad. According to the BD equations (5), interactions should modify the distributions in the following ways: In the limit (i), the sharp distribution shifts to smaller mean values due to the repulsive pressure from the environment. However, in contrast to the entropic model where $f_\sigma^{\mathrm{single}} \to 0$ for $T_\sigma \to 0$, the interaction with the energetic parent does not vanish and still counteracts the outside pressure. Hence, a sharp size distribution with nonvanishing mean for all studied densities will be established. In the limit (i), the parent distribution strictly goes to a Dirac δ function but should be slaved by the position fluctuations of the environment. We conclude tentatively that limit (i) in the energetic model converges to an equilibrium system with a rather monodisperse size distribution with a small polydispersity remaining due to the thermal bulk translational fluctuations.

Conversely, in the limit (ii), $T_\sigma \to \infty$, the size σ becomes a highly fluctuating entity ignoring all (internal and external) forces. Here we thus have a diverging polydispersity and in addition to the broadening size distributions, RDFs are expected to flatten out because there is no well-defined spatial correlation length anymore. However, this is not an ideal gas limit since all particles are still interacting with their instantaneous size. A proper interpretation of this limit is not really clear and, arguably, may not be realizable in experiments because of the physicochemical or geometric bounds of a real system.

C. Simple phenomenological 2T model for $N(\sigma)$

To explain the simulation results of the property distributions $N(\sigma)$ at higher densities a bit more qualitative, we consider a phenomenological model, where interactions between particles and property are considered in terms of a mean (osmotic) pressure from the environment P_0 (with temperature T_0) acting on the one-particle volume V_σ (with temperature T_σ). Since our RCs are compressible, their volume can change under the action of the environment as exemplified by the emergent distributions. Hence, we consider that a particle shrinks in response to the pressure from surrounding particles, and introduce the influence of the pressure through a potential $U_{\mathrm{int}} = P_0V_\sigma$. We assume that in leading order the external pressure comes from the ideal translational contributions and does not depend on the property temperature T_σ. Hence, the pressure can be written as an ideal-gas-like equation of state proportional to temperature in form of $P_0(T_0) = k_BT_0f(\rho\sigma_0^3)$, where we assume f is a function only of density (with $f \to \rho$ in the LDL), not of temperature T_0. The BD equation for the volume of single particle can be written as

$$\zeta_\sigma \dot{V}_\sigma = -k_\sigma(V_\sigma - V_{\sigma,0}) + R_V - P_0(T_0), \tag{9}$$

where $V_{\sigma,0}, k_\sigma$ are the parameters of the confining property potential and R_V is the white noise term. The single-particle reference volume is $V_{\sigma,0} = \pi\sigma_0^3/6$. For small fluctuations of the size around the value σ_0, the volume V_σ can be expressed by a Taylor expansion as $V_\sigma(\sigma) \approx V_{\sigma,0} + \frac{\pi}{2}\sigma_0^2(\sigma - \sigma_0)$. Considering small deviations from the mean, $\dot{V}_\sigma = (\pi/2)\sigma^2\dot{\sigma} \simeq (\pi/2)\sigma_0^2\dot{\sigma}$, then the BD equation for the size σ follows as

$$\zeta_\sigma\dot{\sigma} = -k_\sigma(\sigma - \sigma_0) + \sqrt{2\zeta_\sigma T_\sigma}\eta_\sigma - \frac{2P_0(T_0)}{\pi\sigma_0^2}. \tag{10}$$

Note that this equation is naturally of similar form as the property dynamics in the BD equations (5), only that the pair forces enter as average in the collective pressure term. The stationary probability distribution of (10) for the particle size σ can be immediately written down, via

$$N_{\mathrm{th}}(\sigma) = \frac{1}{Z}\exp\left[-\frac{1}{2}\frac{1}{k_BT_\sigma}\left(k_\sigma(\sigma - \sigma_0)^2 + \frac{4P_0(T_0)\sigma}{\pi\sigma_0^2}\right)\right], \tag{11}$$

TABLE II. Mean σ_0'/σ_0 and standard deviation δ'/σ_0 of the emergent property distributions $N(\sigma)$ for different values T_σ and different densities $\rho\sigma_0^3$ for the entropic model.

	$\rho\sigma_0^3 = 0.02$		$\rho\sigma_0^3 = 0.20$		$\rho\sigma_0^3 = 0.60$		$\rho\sigma_0^3 = 0.95$		$\rho\sigma_0^3 = 1.30$		$\rho\sigma_0^3 = 1.70$		$\rho\sigma_0^3 = 2.0$	
T_σ/T_0	σ_0'/σ_0	δ'/σ_0	σ_0'/σ_0	δ'/σ_0	σ_0'/σ_0	δ'/σ_0	σ_0'/σ_0	δ'/σ_0	σ_0'/σ_0	δ'/σ_0	σ_0'/σ_0	δ'/σ_0	σ_0'/σ_0	δ'/σ_0
0.1	0.95	0.20	0.75	0.20	0.56	0.18	0.47	0.16	0.41	0.16	0.36	0.16	0.32	0.16
0.2	0.97	0.20	0.84	0.20	0.66	0.18	0.58	0.17	0.52	0.16	0.47	0.16	0.44	0.15
0.5	0.98	0.20	0.91	0.20	0.78	0.18	0.70	0.18	0.64	0.17	0.59	0.16	0.56	0.16
1.0	0.98	0.20	0.94	0.20	0.84	0.18	0.77	0.18	0.71	0.17	0.66	0.16	0.63	0.16
2.0	0.98	0.20	0.96	0.20	0.89	0.18	0.83	0.18	0.77	0.17	0.72	0.16	0.69	0.16
5.0	0.98	0.20	0.97	0.20	0.93	0.19	0.88	0.18	0.84	0.17	0.79	0.16	0.75	0.15
10.0	0.98	0.20	0.98	0.20	0.95	0.19	0.92	0.18	0.87	0.17	0.83	0.16	0.80	0.16

which is a function of both T_0 and T_σ. The constant Z is defined through the normalization condition $\int N_{\rm th}(\sigma)\,d\sigma = 1$ and follows as

$$Z = \sqrt{\frac{2\pi k_B T_\sigma}{k_\sigma}}\exp\left[-\frac{2P_0}{\pi}\frac{1}{k_B T_\sigma}\left(1-\frac{P_0(T_0)}{\pi\sigma_0^2 k_\sigma}\right)\right]. \quad (12)$$

In the LDL, the pressure $P_0 \to 0$, and we recover the correct limit for the distribution $N_{\rm th}(\sigma) \to p(\sigma)$.

For the entropic model, the spring constant was defined as $k_\sigma = k_B T_\sigma/\delta_0^2$. Simple algebra shows that the theoretical probability distribution function (11) can be presented as a Gaussian distribution with mean σ_0' that depends on T_σ with a T_σ-independent standard deviation δ', according to

$$\sigma_0' = \sigma_0 - \frac{2P_0(T_0)}{\pi\sigma_0^2}\frac{\delta_0^2}{k_B T_\sigma} \propto T_0/T_\sigma, \quad \delta' = \delta_0. \quad (13)$$

Hence, the shift of the mean size of the emergent distribution is explicitly controlled by the ratio T_0/T_σ.

For the energetic model, the theoretical probability distribution (11) has the parameter $k_\sigma = k_B T_0/\delta_0^2$, independent of T_σ. The same calculation as in the entropic case shows that the probability distribution of σ in this case is now the Gaussian distribution with a mean σ_0' that does not depend on T_σ, while the standard deviation δ' is varying with property temperature T_σ according to the LDL. Hence, we have

$$\sigma_0' = \sigma_0 - \frac{2P_0}{\pi\sigma_0^2}\frac{\delta_0^2}{k_B T_0}, \quad \delta' = \delta_0\sqrt{\frac{T_\sigma}{T_0}}. \quad (14)$$

To compare to the simulations, the values of the mean particle size from simulations for $T_\sigma = T_0$ (from Table II) are fitted with the mean of the theoretical distributions (13) or (14) to find a single effective fit value of P_0 for every density.

We note that the second virial coefficient of our RC system [22] is $B_2/\sigma_0^3 = 1.77$. Hence, the ideal gas assumption used above should be valid for densities $\rho\sigma_0^3 \lesssim 0.56$ above which packing effects dominate. However, since our approach is very qualitative, we have not attempted the more elaborate inclusion of a virial expansion in this paper.

IV. BD SIMULATION RESULTS

A. Emergent distributions in the entropic model

We first discuss the emergent size distributions $N(\sigma)$ of the entropic model. The distributions for very small densities $\rho\sigma_0^3 = 0.02$, approximating the LDL, shown in Fig. 1(a), stay approximately the same for different values of T_σ. This is expected for the entropic model in the LDL, where particles do essentially not interact and we recover the single-particle limit, $N(\sigma) \to p(\sigma)$, recall the discussions around Eq. (4) and in Sec. III A.

For higher densities, for example, $\rho\sigma_0^3 = 0.95$, as shown in Fig. 1(b), colloid-colloid interactions lead to substantial modifications of the curves with T_σ. In equilibrium, $T_\sigma = T_0$, the distributions are shifted to smaller values, simply from the increased packing of the (repulsive) colloids, as we discussed in detail for equilibrium RCs [23]. However, as a feature for ARCs, the mean size of the particles increases (decreases) with increasing (decreasing) σ-temperature, while the standard deviation of the distributions remains essentially constant. This behavior of the size was conjectured already from the limiting thermal behavior discussed in Sec. III A.

TABLE III. Mean σ_0'/σ_0 and standard deviation δ'/σ_0 of the emergent property distributions $N(\sigma)$ for different values T_σ and different densities $\rho\sigma_0^3$ for the energetic model.

	$\rho\sigma_0^3 = 0.02$		$\rho\sigma_0^3 = 0.20$		$\rho\sigma_0^3 = 0.60$		$\rho\sigma_0^3 = 0.95$		$\rho\sigma_0^3 = 1.30$		$\rho\sigma_0^3 = 1.70$		$\rho\sigma_0^3 = 2.0$	
T_σ/T_0	σ_0'/σ_0	δ'/σ_0	σ_0'/σ_0	δ'/σ_0	σ_0'/σ_0	δ'/σ_0	σ_0'/σ_0	δ'/σ_0	σ_0'/σ_0	δ'/σ_0	σ_0'/σ_0	δ'/σ_0	σ_0'/σ_0	δ'/σ_0
0.1	0.98	0.07	0.95	0.07	0.86	0.08	0.79	0.08	0.73	0.08	0.68	0.08	0.65	0.08
0.2	0.98	0.09	0.95	0.09	0.86	0.10	0.79	0.10	0.73	0.10	0.68	0.09	0.65	0.09
0.5	0.98	0.14	0.94	0.14	0.85	0.14	0.78	0.13	0.72	0.13	0.67	0.12	0.64	0.12
1.0	0.98	0.20	0.94	0.20	0.84	0.18	0.77	0.18	0.71	0.17	0.66	0.16	0.63	0.16
2.0	0.98	0.28	0.93	0.27	0.83	0.25	0.75	0.24	0.69	0.23	0.64	0.22	0.61	0.21
5.0	0.98	0.44	0.92	0.42	0.77	0.38	0.70	0.35	0.64	0.33	0.59	0.31	0.56	0.30
10.0	0.99	0.62	0.90	0.57	0.74	0.49	0.65	0.44	0.59	0.41	0.54	0.39	0.51	0.37

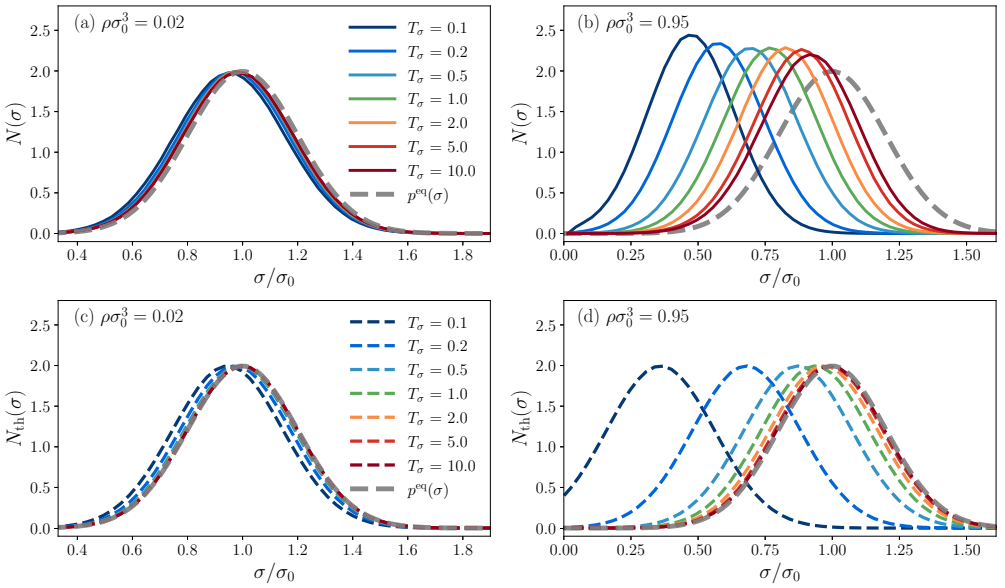

FIG. 1. Property distributions of the "entropic model": emergent distributions $N(\sigma)$ obtained from simulations for two densities [(a) $\rho\sigma_0^3 = 0.02$ and (b) $\rho\sigma_0^3 = 0.95$] fitted with Gaussian distributions (solid lines) compared with the theoretical distributions N_{th} according to the phenomenological model (11) [(c) and (d), dashed lines]. The effective (fit) pressures for the theoretical model are shown in Table IV. The equilibrium parent property distribution $p^{\mathrm{eq}}(\sigma) = p(\sigma; T_\sigma = T_0)$ is presented with a thick gray dashed line as a reference.

The calculated mean and standard deviations for all studied densities are summarized in Table II.

We now describe the trends by our phenomenological model as presented in Sec. III C. The values of the mean particle size from simulations for $T_\sigma = T_0$ (from Table II) were fitted with the mean of the theoretical distribution (13) to find a single effective fit value of P_0, summarized for every density in Table IV. The theoretical trends of $N_{\mathrm{th}}(\sigma)$ for variation of the property temperature T_σ are plotted in Fig. 1(c) and Fig. 1(d) to compare with the simulation results. As we see, the simulation trends can be reproduced by the phenomenological model qualitatively, in particular the substantial shift of the distributions towards larger sizes for increasing T_σ for the high density in Fig. 1(d) are captured very well. We can interpret the results in a way such that the internal temperature T_σ controls the resistance of the internal elasticity to the outside pressure. A "cold" property is squeezed to small values by the external "warmer" pressure more easily, while a "hot" property resists more (like a hot gas) and is expected to approach the single-particle parent distribution, $p(\sigma)$ for $T_\sigma \to \infty$.

The behavior of the emergent size distributions with internal temperature also has interesting consequences on the emergent packing fraction, which we define as $\eta(\rho) = (\pi/6)\langle\sigma^3\rangle\rho$ [23], where $\langle\cdot\rangle$ denote averages in the simulations and $(\pi/6)\langle\sigma^3\rangle$ is the emergent particle volume. The emergent packing as function of system density, $\eta(\rho)$, is presented in Fig. 2. For very low densities, the emergent packing fraction naturally coincides with the nonresponsive expectation linear in density, $\eta_0(\rho) = (\pi/6)\sigma_0^3\rho \propto \rho$ (dashed black line). For higher densities, $\eta(\rho)$ increases sublinear because of the elastic compression of the particle volume, $\langle\sigma^3\rangle(\rho)$, and at some point the curves experience plateau regimes for intermediate values of T_σ, in particular for the cold internal temperatures. As predicted qualitatively by our phenomenological model and the trends discussed for the thermal limits, the value of the packing fraction increases with the σ temperature T_σ due to the larger mean particle sizes for a hot property.

We now turn to the colloidal pair structure in the entropic model: the obtained RDFs are presented in

TABLE IV. Values of the effective pressure parameter P_0 fitted for different densities $\rho\sigma_0^3$ for the entropic model in the phenomenological model; cf. Sec. III C. P_0 has units of $\beta\sigma_0^3$.

$\rho\sigma_0^3$	0.02	0.2	0.6	0.95	1.3	1.7	2.0
P_0	0.2	1.1	2.0	2.5	2.8	3.1	3.3

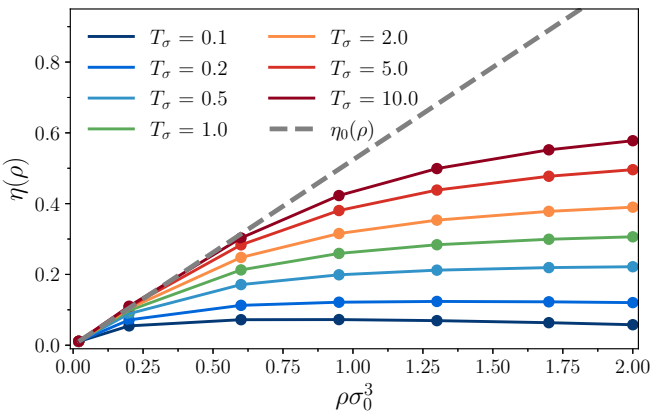

FIG. 2. Dependence of the effective packing fraction $\eta = \rho\frac{\pi}{6}\langle\sigma^3\rangle$ on the density of the system $\rho\sigma_0^3$ for different values of the property temperature T_σ for the entropic model (symbols). Lines are guide to the eye. The (nonresponsive) intrinsic packing fraction, $\eta_0(\rho) = \rho\frac{\pi}{6}\sigma_0^3$, is shown as linear (dashed) gray line.

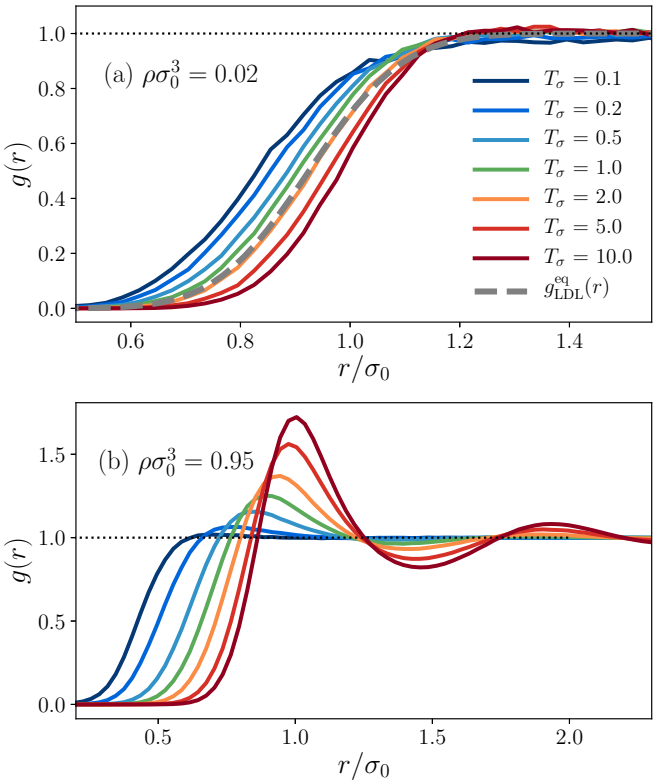

FIG. 3. Radial distribution function (RDF) $g(r)$ of the entropic model varying with property temperature T_σ for densities (a) $\rho\sigma_0^3 = 0.02$ and (b) $\rho\sigma_0^3 = 0.95$. The theoretical solution in the LDL in equilibrium $g^{\rm eq}_{\rm LDL}(r) = \int d\sigma \int d\sigma' p_0(\sigma) p_0(\sigma') \exp[-\phi(r,\sigma,\sigma')/k_B T_0]$ [22] is shown in (a) as a gray dashed line.

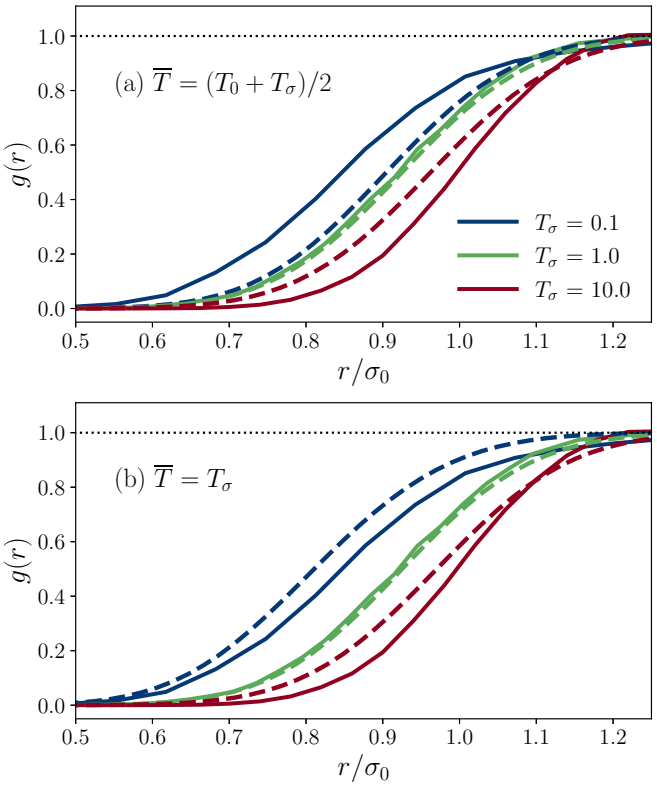

FIG. 4. RDFs for the entropic model obtained in the simulation for $\rho\sigma_0^3 = 0.02$ and selected internal temperatures (solid lines, see legend) compared with the theoretical curves in the LDL $\bar{g}_{\rm LDL}(r) = \int d\sigma \int d\sigma' p_0(\sigma) p_0(\sigma') \exp[-\phi(r,\sigma,\sigma')/k_B \overline{T}]$ (dashed lines) for different effective translational temperatures (a) $\overline{T} = (T_0 + T_\sigma)/2$ and (b) $\overline{T} = T_\sigma$.

Fig. 3. For very low densities [see Fig. 3(a) for $\rho\sigma_0^3 = 0.02$] the RDFs are close to the expected theoretical LDL in equilibrium (i.e., $T_\sigma = T_0$), defined as $g^{\rm eq}_{\rm LDL}(r) = \int d\sigma \int d\sigma' p_0(\sigma) p_0(\sigma') \exp[-\phi(r,\sigma,\sigma')/k_B T_0]$ [22]. However, there is a noticeable variation with property temperature T_σ; in systems with smaller property temperature T_σ the distributions are noticeably shifted to smaller distances than for the higher T_σ. This effect is nontrivial and interesting because the emergent distributions [see Fig. 1(a) again] are hardly affected by T_σ. We suspect this to be a consequence of a two-particle interaction with a high mechanical imbalance, as already implicated by $\dot{\sigma} = f_\sigma^{\rm pair}$, when we discussed the thermal limiting behavior $T_\sigma \to 0$ in Sec. III A. The system thus behaves very volatile for low internal temperatures, highly sensitive to even small perturbations from the environment.

In fact, similar observations were reported in previous works on coupled two-temperature-models [35,42,44], where steady-state energy fluxes between the DoFs coupled to different thermostats were reported. Interestingly, an effective temperature $\bar{T} = \bar{T}(T_0, T_\sigma)$—its details being specific to the particular system—could describe stationary Boltzmann-like distributions of the nonequilibrium system. Inspired by this, and in the absence of a full microscopic theory yet, we plot a hypothetical stationary distribution $\bar{g}_{\rm LDL}(r) = \int d\sigma \int d\sigma' p_0(\sigma) p_0(\sigma') \exp[-\phi(r,\sigma,\sigma')/k_B \bar{T}]$, where we phenomenologically try the effective temperatures $\bar{T} = (T_0 + T_\sigma)/2$ as determined for a symmetric two-particle system previously [35] and simply $\bar{T} = T_\sigma$ in Figs. 4(a) and 4(b), respectively. While both choices display the correct qualitative behavior, the second choice $\bar{T} = T_\sigma$ performs quantitatively better indicating an effective temperature, if definable, closer to the internal temperature.

For higher densities [see Fig. 3(b)] the packing between the particles leads to spatial correlations in the RDFs, however, which are substantially tuneable by the internal temperature T_σ. In the case of decreasing T_σ, the RDFs become flat with a decreasing excluded volume hole. As discussed in Sec. III A, we expect the system to approach ideal-gas-like behavior for $T_\sigma \to 0$ and indeed see the signatures here. In the case of higher T_σ, the "hot" size leads to enhanced packing correlations. As discussed in Sec. III A, for increasing T_σ the emergent distributions [cf. Fig. 1(b)] return to their parent distributions and feature a much larger mean size. The RDFs thus represent in very good agreement those of an equilibrium conventional polydisperse system [23].

B. Emergent distributions in the energetic model

We now discuss the results for the emergent distributions in the energetic model. For the lowest studied density [cf. Fig. 5(a)] the mean value of the property distribution does not change, while the standard deviation increases

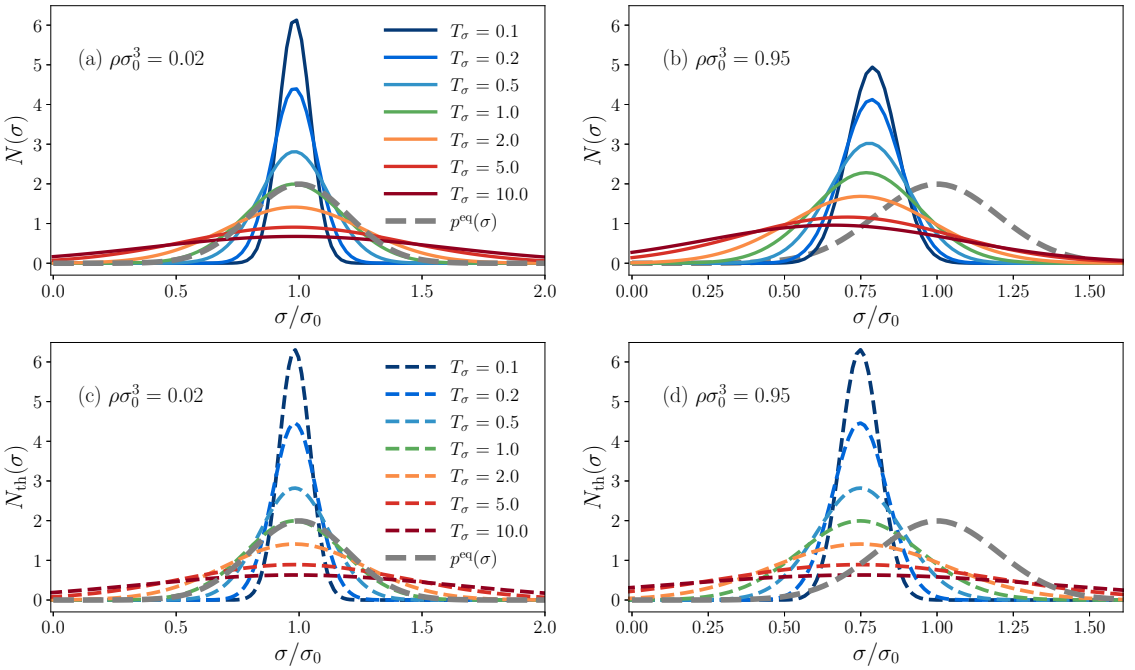

FIG. 5. Property distributions of the "energetic model": emergent distributions $N(\sigma)$ obtained from simulations for two densities [(a) $\rho\sigma_0^3 = 0.02$ and (b) $\rho\sigma_0^3 = 0.95$] fitted with Gaussian distributions (solid lines) compared with with N_{th}, calculated according to the theoretical model (11) [(c) and (d), dashed lines]. The effective (fit) pressures for the theoretical model are shown in Table V. The equilibrium parent property distribution in (a) $p_0^{\mathrm{eq}}(\sigma) = p_0(\sigma; T_\sigma = T_0)$ is presented with a thick gray dashed line as a reference.

substantially with property temperature T_σ: as discussed for the single-particle Boltzmann distributions in Eq. (4), varying the property temperature leads to a variation of the standard deviation according to the law $\delta' = \sqrt{T_\sigma/T_0}\delta_0$. Hence, for large T_σ the (parent) distribution becomes very broad and soft. Interestingly, the qualitative behavior of the standard deviations for both the entropic and energetic models in dependence of T_σ seems not altered by increasing density and interactions; in the energetic model, however, the standard deviations is increasing less strongly with T_σ for dense systems as for the dilute systems.

For higher densities, as exemplified in Fig. 5(b), the pairwise interactions lead to a decreasing mean size, which is dominantly a compression effect as discussed before. Moreover, the standard deviation of the emergent property distribution, $N(\sigma)$, changes in an interesting manner with ρ. For the low property temperatures ($T_\sigma = 0.1$ and 0.2) it can be read off in Table III that it is approximately constant for different densities. On the other hand, for higher values of T_σ, the size distributions is broader for dilute systems and becomes narrower for the denser cases. In other words, the resistance of hot properties to the external stress seems more than counterbalanced by the increasing softness of the distribution, and, in contrast to the entropic case hotter properties do not shift back the distributions to the parent distribution.

Our phenomenological theoretical model with external pressure P_0 can be also applied to explain the effect of varying T_σ on the emergent property distributions in the energetic model. We determine again the parameter P_0 by fitting for every density, summarized in Table V, and plot the theoretical predictions for the T_σ behavior in Fig. 5(c) and Fig. 5(d) for the low density $\rho = 0.02\sigma_0^3$ as well as for the high density $\rho = 0.95\sigma_0^3$, respectively. The theoretical curves describe qualitatively well the simulation distributions at high density. In particular, the mean size does hardly depend on the internal temperature.

The corresponding packing fraction values for the energetic model are presented in Fig. 6. In contrast to the entropic model, for small densities and hot properties the emergent packing fraction is higher than the intrinsic value based on the single-particle mean size, due to the broad size distribution [cf. Fig. 5(a)]. For higher densities a plateau region is observed (similar as in the entropic model), where η increases apparently linearly with T_σ. However, in the energetic model the packing fraction of the hot particles is not as high as in the entropic model because of the discussed emergent size behavior featuring very broad distributions at high T_σ.

The RDFs, $g(r)$, for the energetic model are presented in Fig. 7. For very low densities, Fig. 7(a), we recover the theoretical LDL limit in equilibrium for $T_\sigma = T_0$. In contrast to the entropic model, however, the $g(r)$s have a strong dependence on T_σ because the emergent distributions significantly change with internal temperature in the energetic model. Thus, in strong contrast to the entropic model, in the energetic model the nonequilibrium structure in the LDL is mostly dominated by the parent size distributions and the asymmetrical thermal

TABLE V. Values of the effective pressure P_0 fitted for different densities $\rho\sigma_0^3$ for the energetic model. P_0 has units of $\beta\sigma_0^3$.

$\rho\sigma_0^3$	0.02	0.2	0.6	0.95	1.3	1.7	2.0
P_0	0.7	2.6	7.0	9.9	12.2	14.2	15.4

TABLE VI. Ratios of the diffusion coefficients D_s/D_l and Gaussian relaxation times τ_s/τ_l between 10% of the smallest particles (D_s, τ_s) and 10% of the largest particles (D_l, τ_l) of the system for entropic model. The times τ_i are calculated from autocorrelations of $\sigma(t)$ [23].

	$\rho\sigma_0^3 = 0.02$		$\rho\sigma_0^3 = 0.20$		$\rho\sigma_0^3 = 0.60$		$\rho\sigma_0^3 = 0.95$		$\rho\sigma_0^3 = 1.30$		$\rho\sigma_0^3 = 1.70$		$\rho\sigma_0^3 = 2.0$	
T_σ	D_s/D_l	τ_s/τ_l	D_s/D_l	τ_s/τ_l	D_s/D_l	τ_s/τ_l	D_s/D_l	τ_s/τ_l	D_s/D_l	τ_s/τ_l	D_s/D_l	τ_s/τ_l	D_s/D_l	τ_s/τ_l
0.1	2.15	1.04	2.60	1.00	3.29	0.80	3.70	0.81	4.51	0.67	5.82	0.41	6.50	0.26
0.2	2.10	1.13	2.40	0.96	2.83	0.93	3.05	0.98	3.36	0.85	3.52	0.87	3.86	0.82
0.5	2.09	1.07	2.19	1.13	2.39	1.11	2.50	1.17	2.63	1.06	2.67	1.12	2.8	1.14
1.0	2.09	1.05	2.12	1.14	2.24	1.15	2.30	1.17	2.45	1.19	2.47	1.27	2.57	1.31
2.0	2.09	1.04	2.05	1.12	2.07	1.18	2.16	1.29	2.27	1.31	2.28	1.42	2.29	1.32
5.0	2.09	1.03	2.09	1.14	2.07	1.25	2.05	1.41	2.13	1.42	2.13	1.53	2.18	1.61
10.0	2.09	1.03	2.09	1.10	2.03	1.32	2.01	1.41	2.00	1.49	2.07	1.47	2.01	1.67

couplings between size and position DoFs are secondary. As a consequence, for the higher density $\rho = 0.95\sigma_0^3$ [Fig. 7(b)] the structure behaves very differently, almost oppositely, than in the entropic model. While for smaller T_σ the RDFs exhibit more structure, for higher values of T_σ, the RDF shape is smoother and the rise of $g(r)$ starts at smaller distances r between particles. The behavior of the RDFs can be again explained by the emergent property distributions and the thermal limits discussed in Sec. III B. In the cold property systems, the sizes of the particles are distributed in a very narrow range which leads to a steep increase of $g(r)$. Conversely, in the hot property systems, σ distributes in a wide range and the RDF rises less steep due to the high polydispersity of particles. This effect is more dominant than the high internal resistance as observed for hot properties in the entropic model.

C. Translational diffusion

We finally discuss the emerging translational diffusion behavior of the ARCs. We calculate the long-time self-diffusion constant by standard positional mean-square displacements. We find them to be normal diffusive and thus employ the Einstein relation as in our previous work [23]. Tables VI and VII show that the spread of diffusion (as well as internal relaxation times) between the 10% smallest and 10% largest particles can be tuned over one order of magnitude by varying the internal temperature. Strikingly, we find that the dependence of the diffusion coefficients on the property temperature, $D(T_\sigma)$, shows very different qualitative behavior for the entropic model [see Fig. 8(a)] and the energetic model [see Fig. 8(b)].

In the entropic model, the diffusion constant is a monotonically decreasing function of T_σ for every density. Thus, the hotter the internal property, the slower it becomes translationally. However, diffusion increases with density for cold properties while the opposite is observed for hot properties. The reason can be understood relatively easily from the emergent, density- and T_σ-dependent distributions [see Fig. 1(b) and Table II]. The compression of the size for higher densities and cold properties leads to a highly diminished Stokes friction according to $\zeta_\mathbf{r} = \zeta_0\sigma(t)/\sigma_0$, hence significantly increased diffusion is observed when compared to the isolated particle. However, for hot properties the large particle size leads to a higher Stokes friction and larger packing fractions (cf. Fig. 6). Hence, strong crowding leading to slow diffusion is observed. Remarkable is the strong influence of varying T_σ on the density dependence of the diffusion when compared to equilibrium, $T_\sigma = T_0$, where all curves for different densities mostly collapse due to cancellation of size compression and packing effects [23].

The diffusion in the energetic model behaves very differently. The common trend for every density including the LDL is that the diffusion coefficient rises with property temperature. For low densities ($\rho\sigma_0^3 = 0.02$) there are hardly any particle-particle interactions and the increase of the diffusion coefficient with T_σ is only due to the widening of the emergent property distribution. For comparison we calculate a theoretical mean diffusion value in the LDL by

$$\overline{D} = \int \frac{k_B T_0}{\zeta_0}\frac{\sigma_0}{\sigma} p_0(\sigma)\, d\sigma = D_0\sigma_0\langle\sigma^{-1}\rangle_p, \tag{15}$$

plotted as black dashed line in Fig. 8(b). As we see, the theoretical mean diffusion describes the trend in the LDL very well. In contrast to the entropic model [cf. black dashed line in Fig. 8(a)], hence, the consequence of the property distribution

TABLE VII. Same as Table VI for the energetic model.

	$\rho\sigma_0^3 = 0.02$		$\rho\sigma_0^3 = 0.20$		$\rho\sigma_0^3 = 0.60$		$\rho\sigma_0^3 = 0.95$		$\rho\sigma_0^3 = 1.30$		$\rho\sigma_0^3 = 1.70$		$\rho\sigma_0^3 = 2.0$	
T_σ	D_s/D_l	τ_s/τ_l	D_s/D_l	τ_s/τ_l	D_s/D_l	τ_s/τ_l	D_s/D_l	τ_s/τ_l	D_s/D_l	τ_s/τ_l	D_s/D_l	τ_s/τ_l	D_s/D_l	τ_s/τ_l
0.1	1.26	1.53	1.33	1.74	1.39	1.60	1.42	1.60	1.46	1.39	1.50	1.17	1.53	1.15
0.2	1.38	1.33	1.45	1.32	1.51	1.28	1.52	1.15	1.57	1.06	1.60	1.32	1.57	1.11
0.5	1.65	1.20	1.70	1.02	1.79	1.05	1.86	1.14	1.86	1.27	1.94	1.19	1.94	1.06
1.0	2.09	1.05	2.13	1.14	2.24	1.15	2.30	1.17	2.45	1.19	2.47	1.27	2.57	1.31
2.0	2.93	1.03	3.12	1.01	3.15	1.10	3.34	1.12	3.59	0.98	3.70	1.00	3.93	0.96
5.0	5.87	0.42	5.94	0.45	6.55	0.39	6.55	0.39	6.72	0.36	7.08	0.33	7.58	0.26
10.0	9.38	0.17	9.31	0.17	10.42	0.14	10.45	0.13	9.71	0.15	10.23	0.13	9.69	0.13

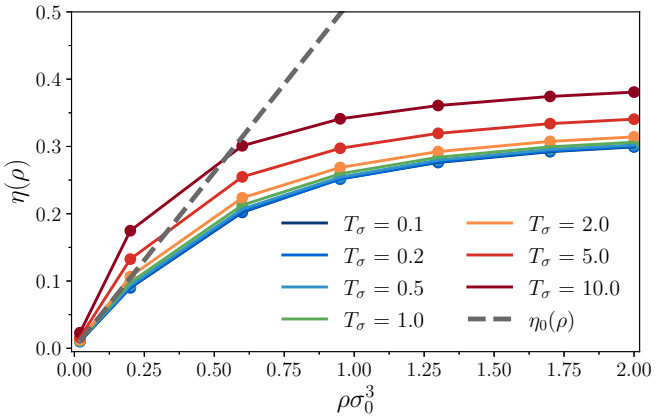

FIG. 6. Dependence of the packing fraction $\eta = \rho\frac{\pi}{6}\langle\sigma^3\rangle$ on the density of the system $\rho\sigma_0^3$ for different values of the property temperature T_σ for the energetic model (symbols). Lines serve as guide to the eye. The intrinsic (nonresponsive) packing fraction $\eta_0 = \rho\frac{\pi}{6}\sigma_0^3$ has a linear dependence (dashed line).

widening is the increase of the mean particle diffusion $\overline{D}$ with property temperature, because small sizes in the wider distribution dominate the transport process. Increasing the density appears to enhance this effect for large $T_\sigma \gg T_0$ because the distributions [cf. again Fig. 5(c)] are shifted to smaller sizes. For small $T_\sigma < T_0$ the trend with density is not so clear; here

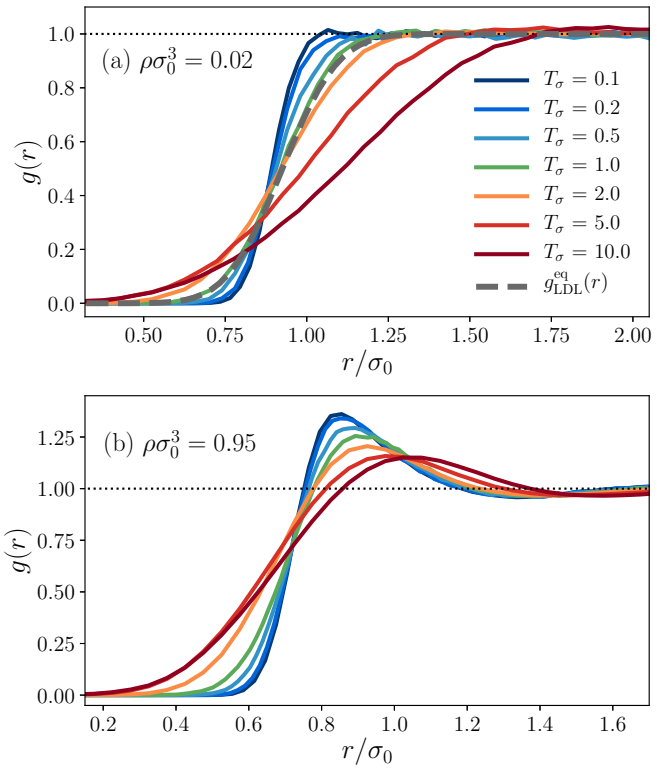

FIG. 7. The RDFs, $g(r)$, of the energetic model with property temperature T_σ for densities (a) $\rho\sigma_0^3 = 0.02$ and (b) $\rho\sigma_0^3 = 0.95$. In (a) we compare with the theoretical LDL solution in equilibrium, $g_{\mathrm{eq}}(r) = \int d\sigma \int d\sigma' p_0(\sigma)p_0(\sigma')\exp[-\phi(r,\sigma,\sigma')/k_BT_0]$ (gray dashed line).

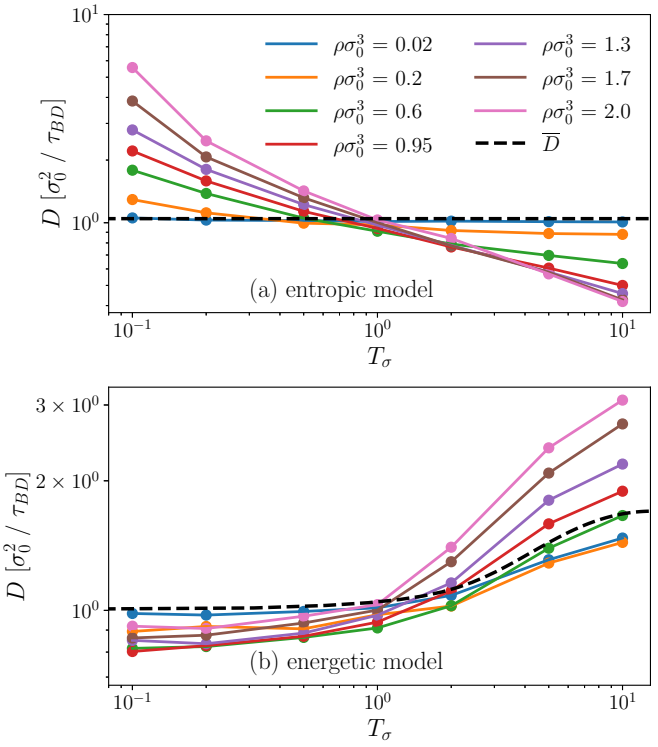

FIG. 8. The dependence of the long-time translational self-diffusion coefficient $D(T_\sigma)$ on the property temperature T_σ for different densities $\rho\sigma_0^3$ for (a) the entropic model and (b) the energetic model (symbols). Solid lines are guide to the eye. The theoretical mean diffusion for the low-density (single-particle) limit, defined as in Eq. (15), is depicted by the black dashed lines.

the size distributions are stiffer and the fluid more structured. Hence, we believe local packing might have some subtle effects on the diffusion, absent in the much smoother "hot" internal system. The smoothing of the energy landscape and the rising diffusion for increasingly dense systems for hot internal temperatures is a very remarkable finding from our point of view.

Finally, it is instructive for our size-fluctuating models to test the validity of the Stokes-Einstein relation, that is, we ask if diffusion is proportional to inverse size of the particles. Since we need to average over a reasonable long-time window for the determination of diffusion we need to average the size. Here, the question appears, if we should average over a mean size or over the mean of inverse size, which are in general different [23]. In Fig. 9 we plot the diffusion constant versus either $\langle\sigma_0/\sigma\rangle$ or $\sigma_0/\langle\sigma\rangle$ for both the entropic and energetic models. Stokes-Einstein naively suggests that the diffusion should be proportional to $\sigma_0/\langle\sigma\rangle$, while one could also suspect a mean diffusion proportional $\langle\sigma_0/\sigma\rangle$ to be applicable, as we have shown in Fig. 8(b) for the energetic model in the dilute density limit. As we see below, a Stokes scaling is not strictly applying, especially not for the energetic model where the emergent distributions can become very broad and are more temperature- and density-dependent as for the entropic model. Here, as mentioned above, in the dilute limit the concept of a mean diffusion seems to apply. For higher densities, non-Stokesian interaction effects also come into play [56]. Hence,

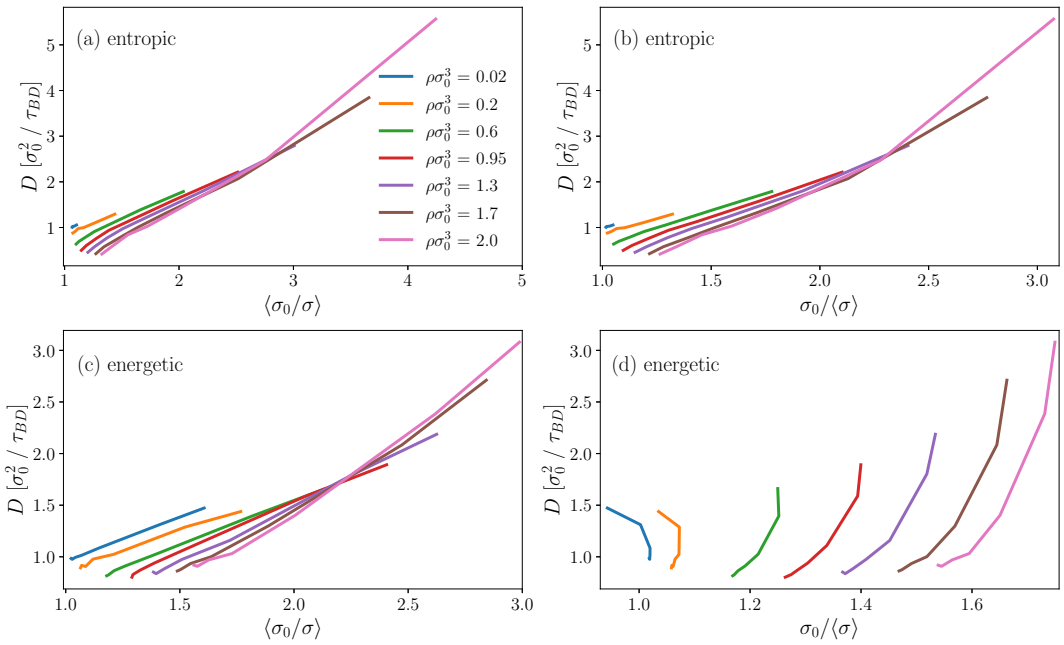

FIG. 9. Test of the Stokes-Einstein relation. Plotted are the diffusion constants vs $\langle\sigma_0/\sigma\rangle$ and $\sigma_0/\langle\sigma\rangle$ for the entropic [(a) and (b)] and energetic model [(c) and (d)], respectively.

the trends cannot be clearly categorized as Stokesian. Recall also that we are dealing here with a nonequilibrium system, so even free volume concepts may not be as applicable as in simple liquids in equilibrium. In [23] we found indications that also the timescale of the internal fluctuations may play a role in diffusion, i.e., if the particles changes size quickly or not when diffusing over their own size.

V. CONCLUDING REMARKS

To summarize, we introduced in this work a model for active responsive colloids (ARCs) to move one step forward into modeling nonequilibrium colloid dispersions with internal activity and "living" properties, such as adaptive and autonomous functional behavior. In here, we found a rich behavior for the structure and dynamics of dispersions of the ARCs controlled by the internal activity ("coldness" or "hotness" of the internal DoF). The results depend substantially on whether the internal DoF is energetic or entropic, i.e., if parent property distributions are affected by the internal "heat engine" or not, respectively. It will be intriguing to find out in future how this relates to specific synthetic active systems and what are then the consequences for material synthesis.

We believe that the findings are quite general in terms of the interaction potential and should hold at least for all simple repulsive pair potentials, including the hard sphere limit. (Note that, of course, the isolated, single-particle size distributions are not affected by the choice of pair potential.) As a support, in Ref. [24] (see Fig. 6 there), we showed using perturbation theory that qualitative trends of the emerging distributions are preserved for softer and harder repulsive pair potentials, including the hard sphere limit.

It is interesting to speculate about possible experimental realizations of entropic versus energetic internal energy landscapes. Since many relevant systems are based on polymer architectures (see [12,36,37,39]), the crucial point is the solution behavior of the polymers. Here we can distinguish between UCST (upper critical solution temperature) and LCST responsive polymers (lower CST) [9], former having a more energetic nature while the latter respond more entropically. In other words, UCST polymers swell with increasing temperature and LCST polymer collapse with increasing temperature. In practice, it is difficult to synthesize purely energetic and entropic polymers in experiments and thus their nature will be always mixed and details dependent on conditions. However, we are elucidating both extremes and give thus meaningful insight about the respective behaviors. Experimental trends tuned by internal activity (e.g., heat of exothermic reaction or by laser light) will thus benefit from the interpretation within our framework.

Our work offers various future applications and extensions and possible questions to address. For example, internal activity in polymodal parent landscapes [24] may give rise to spatiotemporal heterogeneities on different scales and interesting phase behavior due to active switching between conformational states of particles [28,29,58–60]. Moreover, the coupling to external fields (acting on both translation and property) [22] could be interesting with the possibility of localizing active action in space. Furthermore, internal activity may not only be modeled by varying the internal temperature but generally by different forms and types of noise [33]. Fundamentally always the questions arise what are the nonequilibrium thermodynamics, heat and fluxes in such an active system where fluctuation-dissipation theorems hold only in certain limits [35,43,61]. Finally, to move more towards living systems, the missing ingredients in the ARC model are physical descriptions of other biotypical

mechanisms, e.g., such as sensing, communication, and feedback [1–3].

ACKNOWLEDGMENTS

We thank Nils Göth and Michael Bley for useful discussions. J.D. acknowledges support by the state of Baden-Württemberg through bwHPCand the German Research Foundation (DFG) through Grant No. INST 39/963-1 FUGG (bw-ForCluster NEMO) and by the DFG via Grant No. WO 2410/2-1 within the framework of the Research Unit FOR 5099 "Reducing Complexity of Nonequilibrium Systems".

[1] M. Fialkowski, K. J. M. Bishop, R. Klajn, S. K. Smoukov, C. J. Campbell, and B. A. Grzybowski, J. Phys. Chem. B **110**, 2482 (2006).
[2] M. Tena-Solsona, B. Rieß, R. Grötsch, F. Löhrer, C. Wanzke, B. Käsdorf, A. Bausch, P. Müller-Buschbaum, O. Lieleg, and J. Boekhoven, Nat. Commun. **8**, 15895 (2017).
[3] M. B. Miller and B. L. Bassler, Annu. Rev. Microbiol. **55**, 165 (2001).
[4] N. Q. Balaban, J. Merrin, R. Chait, L. Kowalik, and S. Leibler, Science **305**, 1622 (2004).
[5] D. Dubnau and R. Losick, Mol. Microbiol. **61**, 564 (2006).
[6] T. Heuser, E. Weyandt, and A. Walther, Angew. Chem. Int. Ed. **54**, 13258 (2015).
[7] A. Walther, Adv. Mater. **32**, 1905111 (2020).
[8] H. Huang, S. M., A. Petruska, S. Pané, and B. Nelson, Nat. Commun. **7**, 12263 (2016).
[9] M. Stuart, W. Huck, J. Genzer, M. Müller, C. Ober, M. Stamm, G. Sukhorukov, I. Szleifer, V. Tsukruk, M. Urban *et al.*, Nat. Mater. **9**, 101 (2010).
[10] G. Stoychev, N. Puretskiy, and L. Ionov, Soft Matter **7**, 3277 (2011).
[11] S. Fusco, M. S. Sakar, S. Kennedy, C. Peters, R. Bottani, F. Starsich, A. Mao, G. A. Sotiriou, S. Pané, S. E. Pratsinis *et al.*, Adv. Mater. **26**, 952 (2014).
[12] R. Roa, S. Angioletti-Uberti, Y. Lu, J. Dzubiella, F. Piazza, and M. Ballauff, Z. Phys. Chem. **232**, 773 (2018).
[13] K. Kalaitzidou and A. J. Crosby, Appl. Phys. Lett. **93**, 041910 (2008).
[14] G. Wang, Y. Liu, Y. Liu, N. Xia, W. Zhou, Q. Gao, and S. Liu, Colloids Surf. A **529**, 808 (2017).
[15] M. Motornov, R. Sheparovych, R. Lupitskyy, E. MacWilliams, and S. Minko, J. Colloid Interface Sci. **310**, 481 (2007).
[16] P. Padmanabhan and R. Zia, Soft Matter **14**, 3265 (2018).
[17] H. Meng and G. Li, J. Mater. Chem. A **1**, 7838 (2013).
[18] J. Lee, K. H. Ku, C. H. Park, Y. J. Lee, H. Yun, and B. J. Kim, Langmuir **13**, 4230 (2019).
[19] L. A. Lyon and A. Fernandez-Nieves, Annu. Rev. Phys. Chem. **63**, 25 (2012).
[20] R. Keidel, A. Ghavami, D. M. Lugo, G. Lotze, O. Virtanen, P. Beumers, J. S. Pedersen, A. Bardow, R. G. Winkler, and W. Richtering, Sci. Adv. **4**, eaao7086 (2018).
[21] M. Karg, A. Pich, T. Hellweg, T. Hoare, L. A. Lyon, J. J. Crassous, D. Suzuki, R. A. Gumerov, S. Schneider, I. I. Potemkin, and W. Richtering, Langmuir **35**, 6231 (2019).
[22] Y.-C. Lin, B. Rotenberg, and J. Dzubiella, Phys. Rev. E **102**, 042602 (2020).
[23] U. Baul and J. Dzubiella, J. Phys.: Condens. Matter **33**, 174002 (2021).
[24] U. Baul, N. Göth, M. Bley, and J. Dzubiella, J. Chem. Phys. **155**, 244902 (2021).
[25] A. R. Denton and M. Schmidt, J. Phys.: Condens. Matter **14**, 12051 (2002).
[26] M. Urich and A. R. Denton, Soft Matter **12**, 9086 (2016).
[27] S. Ciarella, M. Rey, J. Harrer, N. Holstein, M. Ickler, H. Löwen, N. Vogel, and L. M. C. Janssen, Langmuir **37**, 5364 (2021).
[28] J. Stegen and P. van der Schoot, Soft Matter **11**, 2036 (2015).
[29] J. Stegen and P. van der Schoot, J. Chem. Phys. **142**, 244901 (2015).
[30] I. M. Ilie, W. K. den Otter, and W. J. Briels, J. Chem. Phys. **144**, 085103 (2016).
[31] G. Kapteijns, W. Ji, C. Brito, M. Wyart, and E. Lerner, Phys. Rev. E **99**, 012106 (2019).
[32] L. Berthier, E. Flenner, C. J. Fullerton, C. Scalliet, and M. Singh, J. Stat. Mech.: Theory Exp. (2019) 064004.
[33] P. Romanczuk, M. Bär, W. Ebeling, B. Lindner, and L. Schimansky-Geier, Eur. Phys. J. Spec. Top. **202**, 1 (2012).
[34] C. Bechinger, R. Di Leonardo, H. Löwen, C. Reichhardt, G. Volpe, and G. Volpe, Rev. Mod. Phys. **88**, 045006 (2016).
[35] A. Y. Grosberg and J.-F. Joanny, Phys. Rev. E **92**, 032118 (2015).
[36] C. Wang, X. Liu, V. Wulf, M. Vázquez-González, M. Fadeev, and I. Willner, ACS Nano **13**, 3424 (2019).
[37] I. Aibara, J.-i. Chikazawa, T. Uwada, and S. Hashimoto, J. Phys. Chem. C **121**, 22496 (2017).
[38] S. Merabia, S. Shenogin, L. Joly, P. Keblinski, and J.-L. Barrat, Proc. Natl. Acad. Sci. USA **106**, 15113 (2009).
[39] D. J. Bell, D. Felder, W. G. von Westarp, and M. Wessling, Soft Matter **17**, 592 (2021).
[40] R. Exartier and L. Peliti, Phys. Lett. A **261**, 94 (1999).
[41] D. Rings, R. Schachoff, M. Selmke, F. Cichos, and K. Kroy, Phys. Rev. Lett. **105**, 090604 (2010).
[42] V. Dotsenko, A. Maciołek, O. Vasilyev, and G. Oshanin, Phys. Rev. E **87**, 062130 (2013).
[43] R. R. Netz, Phys. Rev. E **101**, 022120 (2020).
[44] S. N. Weber, C. A. Weber, and E. Frey, Phys. Rev. Lett. **116**, 058301 (2016).
[45] J. Smrek, I. Chubak, C. N. Likos, and K. Kremer, Nat. Commun. **11**, 26 (2020).
[46] A. Y. Grosberg and J. F. Joanny, Polymer Sci. C **60**, 118 (2018).
[47] A. Crisanti, A. Puglisi, and D. Villamaina, Phys. Rev. E **85**, 061127 (2012).
[48] A. Puglisi, A. Sarracino, and A. Vulpiani, Phys. Rep. **709–710**, 1 (2017).
[49] L. Rovigatti, N. Gnan, A. Ninarello, and E. Zaccarelli, Macromolecules **52**, 4895 (2019).

[50] D. Paloli, P. S. Mohanty, J. J. Crassous, E. Zaccarelli, and P. Schurtenberger, Soft Matter **9**, 3000 (2013).
[51] P. S. Mohanty, D. Paloli, J. J. Crassous, E. Zaccarelli, and P. Schurtenberger, J. Chem. Phys. **140**, 094901 (2014).
[52] M. J. Bergman, N. Gnan, M. Obiols-Rabasa, J.-M. Meijer, L. Rovigatti, E. Zaccarelli, and P. Schurtenberger, Nat. Commun. **9**, 5039 (2018).
[53] K. M. Leung, G. Wanger, Q. Guo, Y. Gorby, G. Southam, W. M. Lau, and J. Yang, Soft Matter **7**, 6617 (2011).
[54] E. Yamamoto, T. Akimoto, A. Mitsutake, and R. Metzler, Phys. Rev. Lett. **126**, 128101 (2021).
[55] R. Kubo, Rep. Prog. Phys. **29**, 255 (1966).
[56] J.-P. Hansen and I. R. McDonald, *Theory of Simple Liquids*, 4th ed. (Academic Press, Oxford, 2013) pp. 13–59.
[57] H. J. C. Berendsen, *Simulating the Physical World* (Cambridge University Press, Cambridge, 2007).
[58] A. Moncho-Jordá and J. Dzubiella, Phys. Rev. Lett. **125**, 078001 (2020).
[59] M. Bley, J. Dzubiella, and A. Moncho-Jordá, Soft Matter **17**, 7682 (2021).
[60] M. Bley, P. I. Hurtado, J. Dzubiella, and A. Moncho-Jordá, Soft Matter **18**, 397 (2022).
[61] U. Seifert, Phys. Rev. Lett. **95**, 040602 (2005).